Acta Oceanol. Sin., 2022, Vol. 41, No. 4, P. 14–22
https://doi.org/10.1007/s13131-021-1854-7
http://www.aosocean.com
E-mail: ocean2@hyxb.org.cn

Seasonal and spatial variations of kinematic parameters of internal solitary waves in the Andaman Sea

Yuqi Wu[1, 2, 5], Jieshuo Xie[1, 3], Jiexin Xu[1, 3*], Zhiwu Chen[1, 3], Yinghui He[1, 3], Shuqun Cai[1, 3, 4*]

[1] State Key Laboratory of Tropical Oceanography, South China Sea Institute of Oceanology, Chinese Academy of Sciences, Guangzhou 510301, China

[2] University of Chinese Academy of Sciences, Beijing 100049, China

[3] Southern Marine Science and Engineering Guangdong Laboratory (Guangzhou), Guangzhou 511458, China

[4] Institution of South China Sea Ecology and Environmental Engineering, Chinese Academy of Sciences, Guangzhou 510301, China

[5] Marine Development Planning and Research Center of Guangdong Province, Guangzhou 510220, China

Received 21 January 2021; accepted 17 April 2021

Abstract

The horizontally variable density stratification and background currents are taken into the variable-coefficent extended Korteweg-de Vries (evKdV) theory to obtain the geographical and seasonal distribution of kinematic parameters of internal solitary waves in the Andaman Sea (AS). The kinematic parameters include phase speed, dispersion parameter, quadratic and cubic nonlinear parameters. It shows that the phase speed and dispersion parameter are mainly determined by the topographic feature and have limited seasonal variation. The maximum phase speed is 2.6 m/s, which occurs in the cool season (November) in the middle of the AS, while the phase speed in the cool season is slightly larger than those in other seasons, up to 11.4% larger than that in the rainy season (July) in the southern AS. The dispersion parameter in the cool season can be 22.3% larger than that in the hot season. The nonlinear parameters have significant seasonal variation, and they can even change their signs at the continental slope in the north of the AS, from season to season. Meanwhile, the algebraic solitons dominate in the AS with minimum amplitudes (a_{al}) ranging from 0.1 m to 102 m, and the maximum a_{al} occurs in the cool season in the southern AS. The effect of the background flow on the parameters is also studied. The background flow has a great influence on the nonlinear parameters, e.g., the value of cubic nonlinear parameter can be reduced by 1/3 when the background flow is not considered.

Key words: internal solitary waves, kinematic parameters, evKdV theory, Andaman Sea

Citation: Wu Yuqi, Xie Jieshuo, Xu Jiexin, Chen Zhiwu, He Yinghui, Cai Shuqun. 2022. Seasonal and spatial variations of kinematic parameters of internal solitary waves in the Andaman Sea. Acta Oceanologica Sinica, 41(4): 14–22, doi: 10.1007/s13131-021-1854-7

1 Introduction

Internal solitary waves (ISWs) have been extensively observed by both *in-situ* measurements (Perry and Schimke, 1965; Osborne and Burch, 1980; Hyder et al., 2005) and satellites remote sensing images (Apel et al., 1985; Alpers et al., 1997; da Silva and Magalhaes, 2016; Zhou et al., 2016; Magalhaes and da Silva, 2018; Wang et al., 2019) in the Andaman Sea (AS). Exxon production Research Company conducted an *in-situ* oceanographic measurement program in the southern AS. The measurement showed that ISWs appeared in packets at a frequency of about 12 h and 26 min and the internal wave induced currents can be up to 1.8 m/s (Osborne and Burch, 1980). Hyder et al. (2005) observed eastward propagating ISWs with an amplitude of 60 m in the northeast of the Andaman Islands.

ISWs in the AS occur all year round, but most ISWs are observed by satellite images from February to April (hot season), and following from May to October (rainy season), and the least from November to January (cool season). The spatial distribution of ISWs also shows significant difference. ISWs are mostly observed in the northern Sumatra Island, western Malay Peninsula, Nicobar Islands and northeastern Andaman Islands (Wang et al., 2019). Thus, ISWs in the AS have remarkable spatial and temporal difference. However, the characteristics of ISWs in the AS remain unclear, which is different from the South China Sea, where characteristic parameters has been calculated (Grimshaw et al., 2010; Liao et al., 2014; Kurkina et al., 2017b). What are the

Foundation item: The Key Research Program of Frontier Sciences, Chinese Academy of Sciences under contract No. QYZDJ-SSW-DQC034; the Grant from Southern Marine Science and Engineering Guangdong Laboratory (Guangzhou) under contract No. GML2019ZD0304; the National Natural Science Foundation of China under contract Nos 41521005, 41776007 and 41776008; the Guangdong Natural Science Foundation under contract No. 2020A1515010495; the Grant from Chinese Academy of Sciences under contract No. ISEE2021PY01; the Guangzhou Science and Technology Program under contract No. 201804010373; the Youth Science and Technology Innovation Talent of Guangdong TeZhi Plan under contract No. 2019TQ05H519; the Pearl River S&T Nova Program of Guangzhou under contract No. 201806010091; the Rising Star Foundation of South China Sea Institute of Oceanology under contract No. NHXX2019WL0201; the Youth Innovation Promotion Association of Chinese Academy of Sciences under contract No. 2018378; the State Key Laboratory of Tropical Oceanography Independent Research Program under contract No. LTOZZ2001.
*Corresponding author, E-mail: manglo.xu@163.com; caisq@scsioac.cn

seasonal variation and spatial distribution of the characteristic parameters in the AS? How does the hydrological background influence the characteristic parameters of ISWs? All these problems need to be studied.

Osborne and Burch (1980) concluded that ISWs in the AS can be well described by the Korteweg-de Vries (KdV) theory. The KdV equation was first derived by Benney (1966), providing a basic solution to estimate the weakly nonlinear ISWs characteristics, such as the wave speed, the disperison and nonlinear parameters. However, the nonlinear term in the KdV equation is very small. When the pycnocline lies just in the middle depth of the fluid, the nonlinear term will vanish. Thus the extended KdV (eKdV) equation in which the high-order nonlinear term is considered was derived (Kakutani and Yamasaki, 1978; Lamb and Yan 1996; Grimshaw et al. 2002). Furthermore, since kinematic parameters can be affected by the background flow which can vary in space and time. When the background flow is taken into account, the variable-coefficient extended KdV (evKdV) equation is derived (Zhou and Grimshaw, 1989; Holloway et al., 1999; Grimshaw, 2001; Grimshaw et al., 2004, 2010).

In this paper, based on the evKdV equation, we focus on the geographical distribution and seasonal variation of kinematic parameters of ISWs in the AS, and examine the effects of the variable stratification and background currents on these kinematic parameters. The rest is arranged as follows. The data and theoretical methods are described in Section 2 and Section 3, respectively. The results and discussion of these calculations are presented in Section 4. The conclusions are presented in Section 5.

2 Data

The topographic data used in this study are obtained from ETOPO1 Global Relief Model with a spatial resolution of 1′. The monthly temperature and salinity data with the 0.5°×0.5° horizontal resolution are derived from the Simple Ocean Data Assimilation (SODA) system, version 2.1.6, and have been averaged over decades. The depth of hydrographical data can reach to 5 000 m. The monthly background current data from 2011 to 2018 obtained from the Hybrid Coordinate Ocean model (HYCOM) have been averaged. For convenience, we interpolate the above data so that the resolutions are 0.125°×0.125° horizontally and 5 m vertically, respectively. Figure 1 shows the surface horizontal velocity vectors in the AS in each season. Zhou et al. (2016) collected thousands satellite images and observed that the ISWs mainly propagated along the east-west direction. Therefore, here we only consider the effect of the zonal component of background flow. The surface current velocities vary greatly with seasons. In the hot season (March), the maximum zonal current velocity is 0.32 m/s in the southwest of the AS, whilst in the rainy season (July), the zonal current velocities get larger in the central and northern AS with a maximum of 0.51 m/s, and the current velocity in the cool season (November) is smaller than those in the other two seasons. The maximum zonal current velocity is 0.27 m/s in the north of the AS.

3 Variable-coefficient extended Korteweg-de Vries equation

When the influence of the horizontally variable stratification and background currents have been taken into account, the evKdV equation (Grimshaw et al., 2004) used in this study is as follows:

$$\frac{\partial \eta}{\partial t}+c\frac{\partial \eta}{\partial x}+\alpha\eta\frac{\partial \eta}{\partial x}+\alpha_1\eta^2\frac{\partial \eta}{\partial x}+\beta\frac{\partial^3\eta}{\partial x^3}+\frac{c}{2Q}\frac{\mathrm{d}Q}{\mathrm{d}x}\eta=0, \quad (1)$$

where x is the horizontal coordinate, t is the time; $\eta(x,t)$ is the vertical displacement of the pycnocline; c, β, α and α_1 are the linear phase speed, dispersion parameter, quadratic and cubic nonlinear parameters, respectively. The function $Q(x)$ is the linear amplification factor due to variable depth and horizontally variable hydrology. The phase speed c is determined by the eigenvalue problem for $\Phi(z)$. Under the Boussinesq approximation, the modal equation is as follows:

$$\frac{\mathrm{d}}{\mathrm{d}z}\left\{[c-U(z)]^2\frac{\mathrm{d}\Phi}{\mathrm{d}z}\right\}+N^2(z)\Phi=0, \quad (2)$$

with the boundary conditions $\Phi(0)=\Phi(-H)=0$ and normalized condition $\Phi(z_{\max})=1$, where $z_{\max}$ is negative value of the depth with the maximum value of Φ. $U(z)$ is the background zonal velocity; H is the total water depth; $N(z)=\left(-\frac{g}{\rho}\frac{\mathrm{d}\rho}{\mathrm{d}z}\right)^{1/2}$ is the buoyancy frequency; and ρ is the potential density. Take position

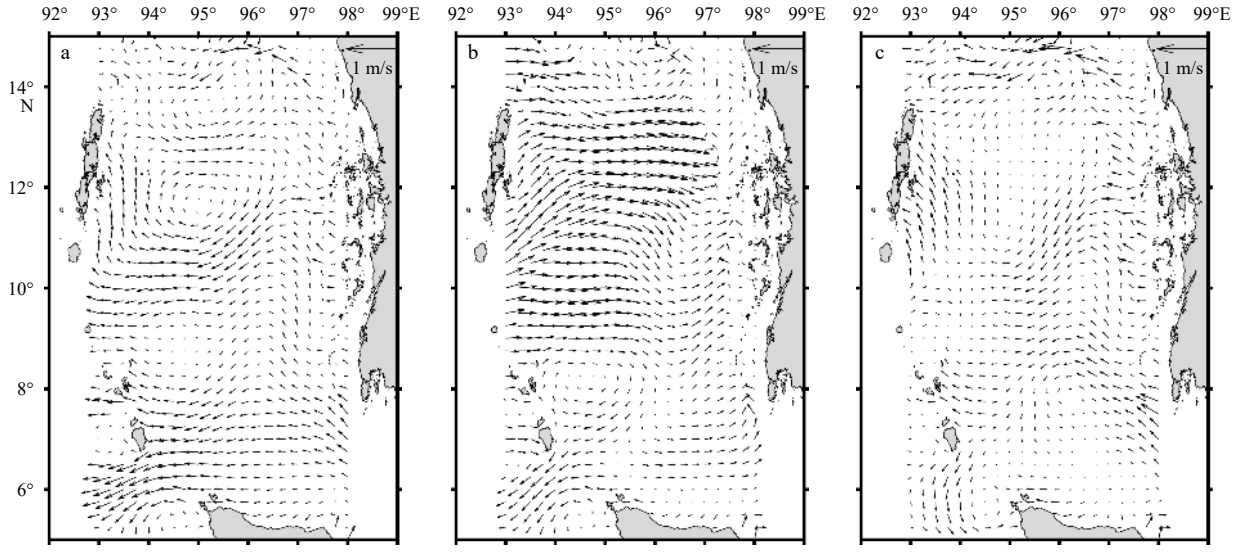

Fig. 1. Multi-year averaged horizontal surface current velocity vectors (unit: m/s) in the Andaman Sea in March (a), July (b) and November (c) from Hybrid Coordinate Ocean model.

6°N, 94°E as an example, the vertical profiles of the potential density and buoyancy frequency in different seasons are shown in Figs 2a and b, respectively. It shows little difference between different seasons. The maximum values of N in July and November both occur at 85 m, whilst the maximum in March occurs at 105 m. The modal Eq. (2) is solved by difference method. Figure 3a presents the solutions of $\Phi(z)$ in different seasons at 6°N, 94°E, where $z_{\max}$ in March, July and November are very close, –640 m, –670 m and –650 m, respectively.

The dispersion, quadratic and cubic nonlinear parameters β, α and α_1 are given by

$$\beta = \frac{1}{2}\frac{\int_{-H}^{0}(c-U)^2\Phi^2\mathrm{d}z}{\int_{-H}^{0}(c-U)\left(\frac{\mathrm{d}\Phi}{\mathrm{d}z}\right)^2\mathrm{d}z}, \tag{3}$$

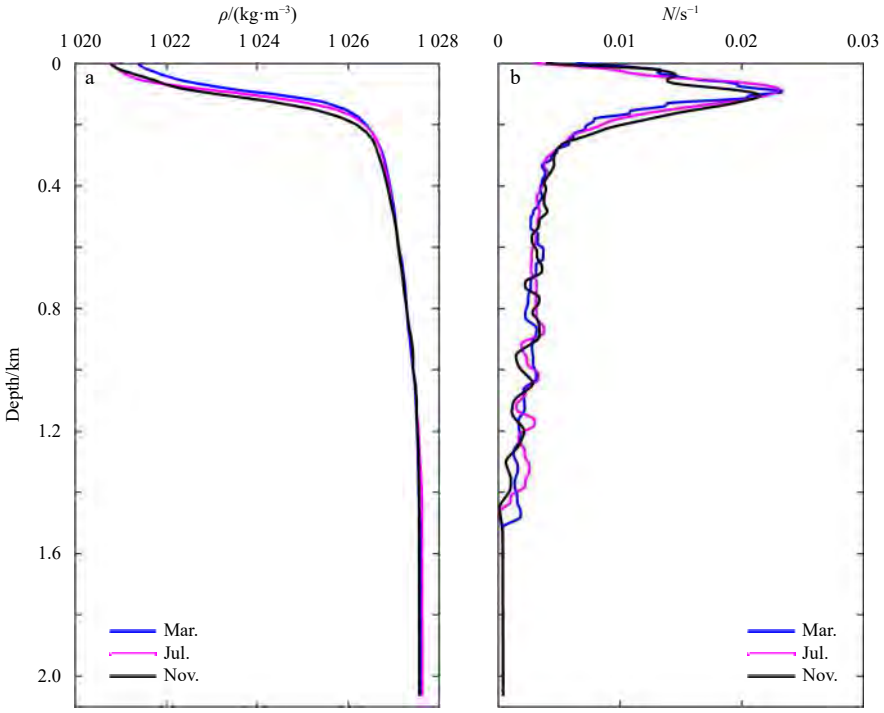

Fig. 2. The vertical profiles of the potential density ρ (a) and buoyancy frequency N (b) at 6°N, 94°E.

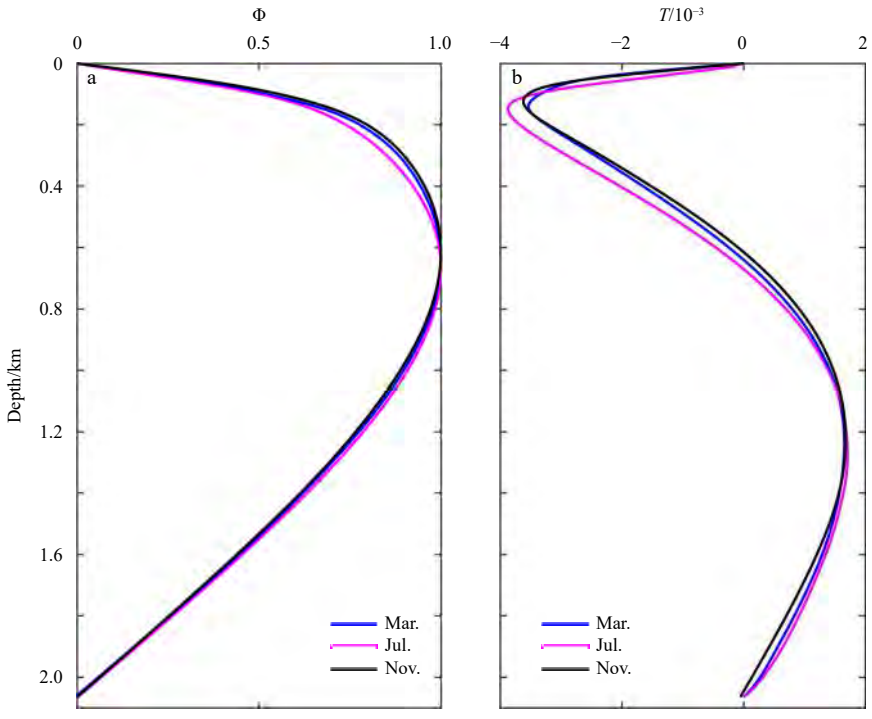

Fig. 3. Numerical solutions of the vertical structures of the model function $\Phi(z)$ (a) and the nonlinear correction $T(z)$ (b) at 6°N, 94°E.

$$\alpha = \frac{3}{2}\frac{\int_{-H}^{0}(c-U)^2\left(\frac{\mathrm{d}\Phi}{\mathrm{d}z}\right)^3\mathrm{d}z}{\int_{-H}^{0}(c-U)\left(\frac{\mathrm{d}\Phi}{\mathrm{d}z}\right)^2\mathrm{d}z}, \tag{4}$$

$$\alpha_1 = \frac{\int_{-H}^{0}(\mathrm{I}+\mathrm{II})\,\mathrm{d}z}{\int_{-H}^{0}(c-U)\left(\frac{\mathrm{d}\Phi}{\mathrm{d}z}\right)^2\mathrm{d}z}, \tag{5}$$

where

$$\mathrm{I} = 9(c-U)^2\frac{\mathrm{d}T}{\mathrm{d}z}\left(\frac{\mathrm{d}\Phi}{\mathrm{d}z}\right)^2 - 4\alpha(c-U)\frac{\mathrm{d}T}{\mathrm{d}z}\frac{\mathrm{d}\Phi}{\mathrm{d}z},$$

$$\mathrm{II} = -\alpha^2\left(\frac{\mathrm{d}\Phi}{\mathrm{d}z}\right)^2 + 5\alpha(c-U)\left(\frac{\mathrm{d}\Phi}{\mathrm{d}z}\right)^3 - 6(c-U)^2\left(\frac{\mathrm{d}\Phi}{\mathrm{d}z}\right)^4.$$

Here $T(z)$ is the nonlinear correction to the modal structure, which can be found as a solution of the following eigenvalue equation:

$$\frac{\mathrm{d}}{\mathrm{d}z}\left[(c-U)^2\frac{\mathrm{d}T}{\mathrm{d}z}\right] + N^2T = -\alpha\frac{\mathrm{d}}{\mathrm{d}z}\left[(c-U)\frac{\mathrm{d}\Phi}{\mathrm{d}z}\right] + \frac{3}{2}\frac{\mathrm{d}}{\mathrm{d}z}\left[\left((c-U)^2\frac{\mathrm{d}\Phi}{\mathrm{d}z}\right)^2\right], \tag{6}$$

with boundary conditions $T(0) = T(-H) = 0$, and the normalized condition $T(z_{\max}) = 0$, where $z_{\max}$ can be found from $\Phi(z_{\max}) = 1$. The vertical structure of $T(z)$ at 6°N, 94°E is shown in Fig. 3b. The isopycnal surface displacement $\zeta(z,x,t)$ is given by

$$\zeta(z,x,t) = \eta(x,t)\,\Phi(z) + \eta^2(x,t)\,T(z). \tag{7}$$

The wave function $\eta(x,t)$ equals to the isopycnal surface displacement at the depth $z_{\max}$. The term Q in Eq. (1) is given by

$$Q = \frac{c_0^2\int_{-H}^{0}(c_0-U_0)\left(\frac{\mathrm{d}\Phi_0}{\mathrm{d}z}\right)^2\mathrm{d}z}{c^2\int_{-H}^{0}(c-U)\left(\frac{\mathrm{d}\Phi}{\mathrm{d}z}\right)^2\mathrm{d}z}. \tag{8}$$

The subscript 0 refers to a reference horizontal position x_0, here we take the grid points at 94°E as the reference points. After the variable substitution,

$$s = \int\frac{\mathrm{d}x}{c(x)} - t, \tag{9}$$

$$\zeta(x,s) = \frac{\eta(x,s)}{Q(x)}, \tag{10}$$

Eq. (1) can be reduced to

$$\frac{\partial\zeta}{\partial x} + \left(\frac{\alpha Q}{c^2}\zeta + \frac{\alpha_1 Q^2}{c^2}\zeta^2\right)\frac{\partial\zeta}{\partial s} + \frac{\beta}{c^4}\frac{\partial^3\zeta}{\partial s^3} = 0. \tag{11}$$

The steady-state solution of Eq. (11) is

$$\zeta = \frac{A}{1+B\cosh\left[\gamma(s-kx)\right]}, \tag{12}$$

where the parameters A, B, k and γ are given by

$$A = \frac{6\beta\gamma^2}{\alpha c^2 Q}, \tag{13}$$

$$\gamma = \sqrt{\frac{\alpha^2c^2}{6\alpha_1\beta}(B^2-1)}, \tag{14}$$

$$k = \frac{\beta\gamma^2}{c^4}. \tag{15}$$

The amplitude of the ISW is determined as

$$a = \frac{A}{1+B} = (B-1)\frac{\alpha}{Q\alpha_1}. \tag{16}$$

Only one parameter in Eq. (12) is arbitrary, and the others can be expressed through it. For $\alpha_1<0$ and $0<B<1$, the polarity of the solitons is determined by the sign of α. In the case $\alpha>0$, the soliton has positive polarity in the "table-top" form. The soliton amplitude is bounded by upper limit,

$$a_{\mathrm{lim}} = -\frac{\alpha}{Q\alpha_1}. \tag{17}$$

For $\alpha_1>0$, there are two branches of ISWs. In the case $\alpha>0$ and $1<B<+\infty$, the amplitude of a solitary wave varies from zero to infinity. When $\alpha<0$ and $-\infty<B<-1$, the ISW has negative polarity, and the absolute value of the ISW amplitude varies from

$$a_{\mathrm{al}} = -\frac{2\alpha}{Q\alpha_1}, \tag{18}$$

to infinity. a_{al} is the minimum amplitude of the ISW.

In the following, we first use evKdV equation with stratification and background currents to calculate the characteristic parameters of ISWs in the AS, then, these parameters are calculated in the case of $U(z)$=0, and the effect of background currents on these parameters is discussed by comparison. Besides, slow variation of the hydrology is assumed in the evKdV theory. In the AS, the stratification and water depth vary slowly in the horizontal direction in most area. Therefore, the evKdV theory is suitable here.

4 Results and discussion

4.1 *Parameters of the linear terms in the evKdV equation*

The phase speed c and dispersion parameter β are two linear parameters in Eq. (1). Their seasonal variation and spatial distribution are shown in Figs 4–7. These parameters are apparently mainly determined by the bathymetry. Seasonal change of stratification has limited impact on them. The maximum phase speed in the AS is 2.6 m/s in the cool season (November), which located in the middle of the AS. From Figs 4a–c, we can see that the seasonal variations of these two linear parameters are almost

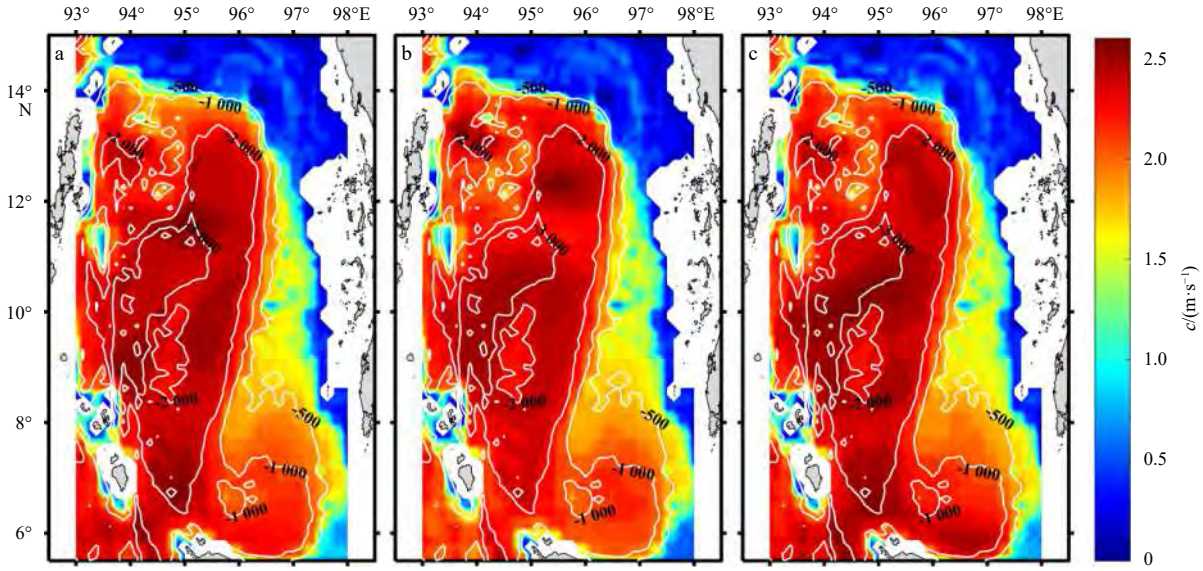

Fig. 4. Geographic distribution of the phase speed c in March (a), July (b) and November (c). The white lines are isobaths in m.

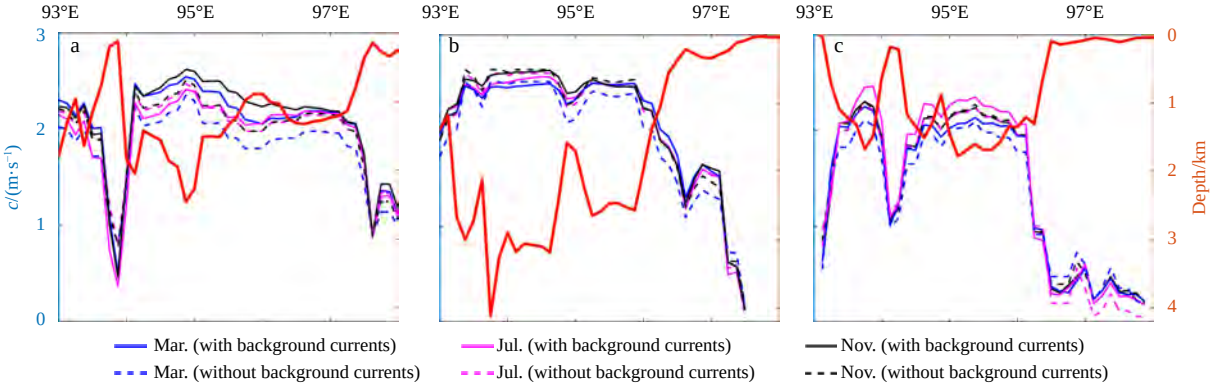

Fig. 5. Zonal distribution of phase speed c obtained by evKdV equation with background currents (solid lines) and without background currents (dashed lines) along the transects of 6.5°N (a), 10°N (b) and 13.5°N (c). The thick red lines represent the bathymetries along the transects.

negligible in the area where the depth is less than 2 000 m. In order to better understand the variation of parameters in various regions of the AS, we select transects 6.5°N, 10°N and 13.5°N to represent the southern, central and northern AS, respectively. Figures 5a–c (solid lines) indicate that the phase speed is the largest in the southern AS and the smallest in the northern AS. The seasonal difference in the phase speed is also the largest in the south. The phase speed in the cool season (November) can be 11.4% larger than that in the rainy season (July). The maximum phase speed occurs in different seasons with different transects. In the southern and central AS, the phase speed is the largest in the cool season, while in the north it is the largest in the rainy season.

The spatial distribution of the dispersion parameter β is also mainly related to topographic feature. The maximum value of β is 5.23×10^5 m^3/s in the rainy season. Figures 6 and 7 show that β in the deep water area, i.e., the central of the AS, have obvious seasonal difference. While in the south and north, the seasonal variation of β is insignificant. In the central region, β in the cool season (November) is the largest, and in hot season (March) is the smallest. β in the cool season can be 22.3% larger than that in the hot season.

The dependence of the linear parameters of ISWs on bathymetry in the AS agrees with the conclusion in the South China Sea (SCS) (Liao et al., 2014). However, in the AS, the phase speed and dispersion parameter are both smaller than those in the SCS, and they show little season variation.

4.2 *Parameters of the nonlinear terms in the evKdV equation*

Compared with linear parameters c and β, the nonlinear parameters α and α_1 are sensitive with background currents and density stratification (Figs 8–11). Their seasonal variations are significant. They can even change their signs at some locations, especially at the continental slope north of the AS, from season to season. This is mainly due to the change of the depth with maximum buoyancy frequency at the continental slope.

The positive extremum of α mainly appear near the continental slopes and islands where bottom topographies change sharply. In the north and east of the AS, from rainy season to cool season, the sign of α changes from positive to negative, i.e. the internal solitary wave deforms from an elevation wave to a depression one. When the depth is larger than 1 000 m, the value of α fluctuates around –0.006 5 s^{-1}. Figures 9a–c show that in the southern and central AS, there is a significant seasonal change in

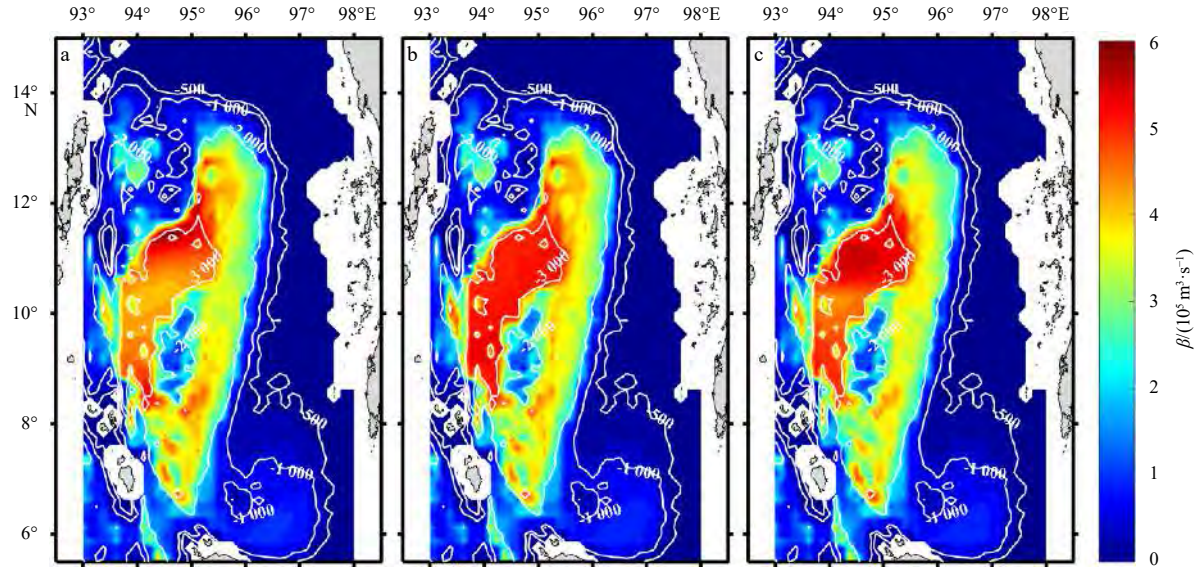

Fig. 6. Geographic distribution of the dispersion parameter β in March (a), July (b) and November (c). The white lines are isobaths in m.

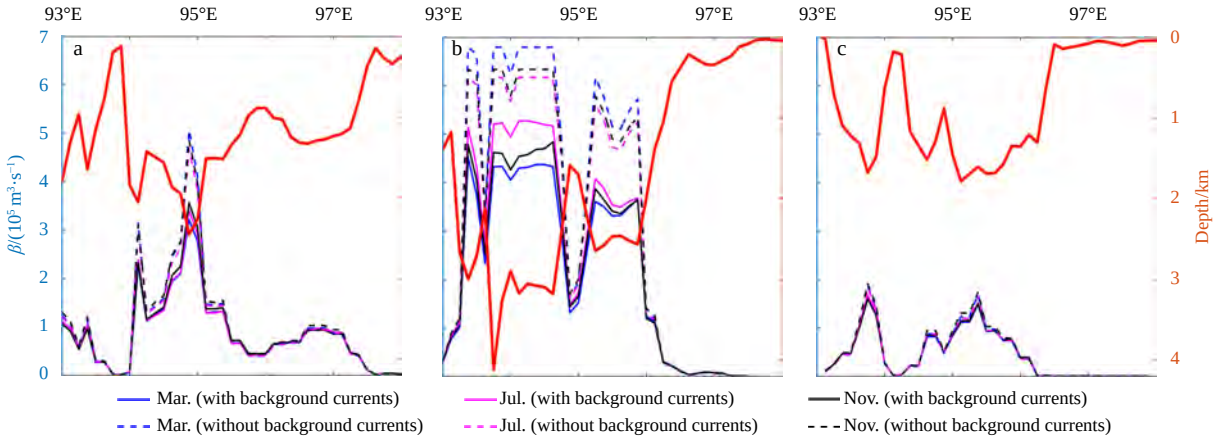

Fig. 7. Zonal distribution of the dispersion parameter β obtained by evKdV equation with background currents (solid lines) and without background currents (dashed lines) along the transects of 6.5°N (a), 10°N (b) and 13.5°N (c). The thick red lines represent the bathymetries along the transects.

α. The value of α in the rainy season is up to 23.3% greater than that in the cool season in the southern AS, and 28.5% greater than that in the hot season in the central AS. In the northern AS, the seasonal variation of α is very small in the deep water area and becomes larger on the continental slope. The value of α is very similar to the result in the SCS (Cai et al., 2014), which fluctuates around –0.006 s^{-1} in deep sea area. However, due to the significant seasonal variation of the density stratification, α shows larger seasonal variation in the SCS.

The quadratic nonlinear term may vanish when the upper layer depth is equal to the lower layer depth in a two-layer fluid, in this case the role of the cubic nonlinear term increases. In the shallow water area, the cubic nonlinear parameter α_1 is negative and its value is smallest in the cool season, which can reach –0.004 4 m/s. In the deep sea, α_1 is positive and the value is the largest in the cool season, which can be up to 0.007 m/s. The seasonal variation is obvious, especially in the central AS (Figs 10 and 11). The value of α_1 in the hot season can be 71.9% larger than that in the rainy season. α_1 in the rainy season are much smaller than those in the other two seasons in the deep water area.

4.3 *Amplitudes of the ISWs in the AS*

The polarity of the ISW is determined by the sign of nonlinear parameters (α, α_1). Note that the negative cubic nonlinear parameters are only present in the shallow water area, the algebraic solitons dominate in the AS. Figure 12 illustrates the geographic distribution of minimum algebraic solitons amplitudes a_{al} in the areas with positive α_1. The larger values are mostly located in the areas with a water depth less than 2 000 m but larger than 1 000 m. This is different from the results in the northern SCS, the Mediterranean Sea and the Black Sea where the larger ones all exist in the areas with a water depth shallower than 1 000 m (Liao et al., 2014; Kurkina et al., 2017a). a_{al} is the largest in the cool season, ranging from 0.1 m to 102 m, and the maximum a_{al} occurs in the southern AS.

4.4 *Effect of background currents*

Figure 1 shows that both speeds and directions of background currents in the AS vary a lot in seasons and space. To figure out the effect of the variable background currents on the seasonal variation and spatial distribution of ISWs in the AS, we

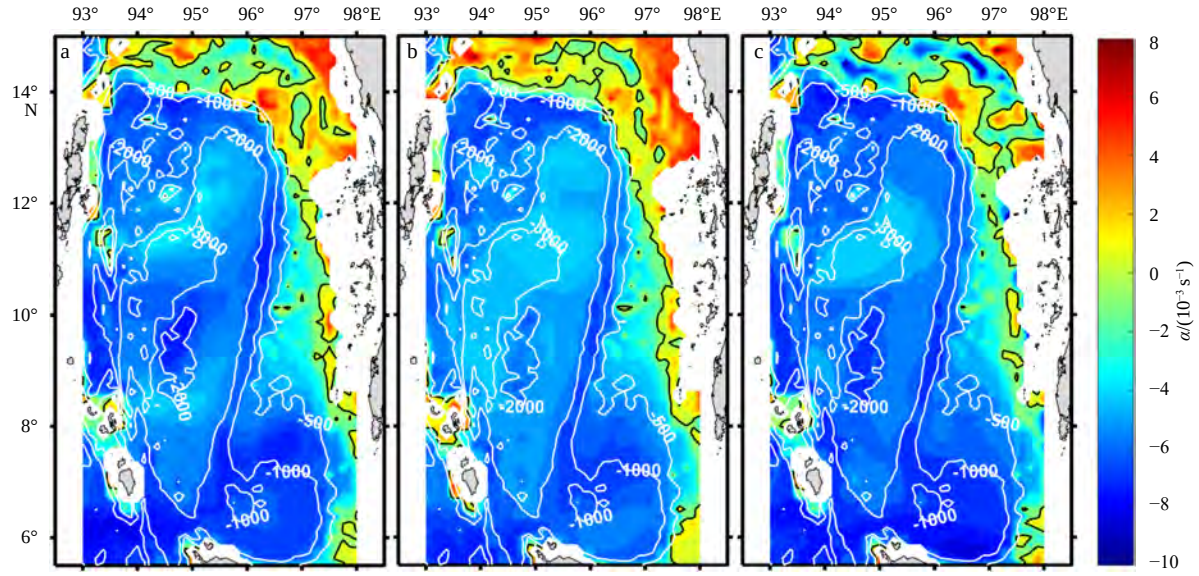

Fig. 8. Geographic distribution of the quadratic parameter α in March (a), July (b) and November (c). The black and white lines are zero contours of α in s^{-1} and isobaths in m, respectively.

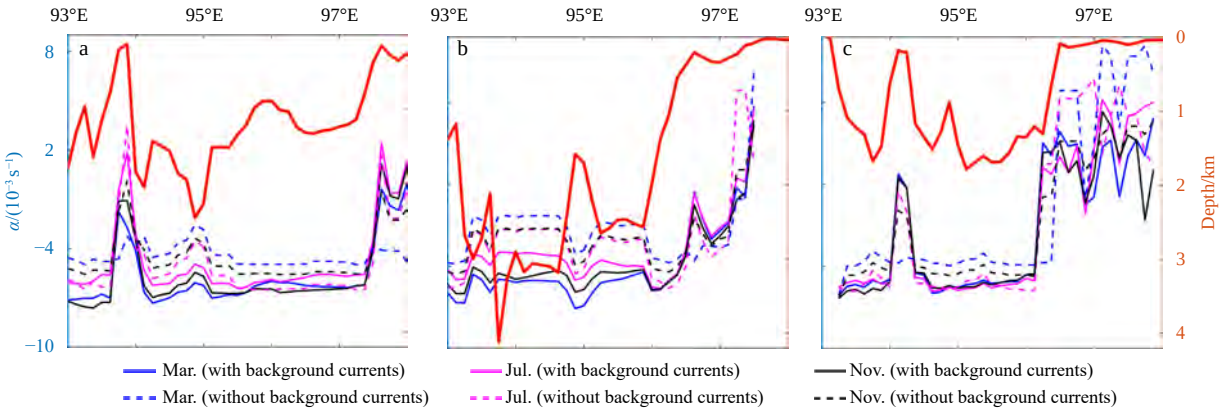

Fig. 9. Zonal distribution of the quadratic parameter α obtained by evKdV equation with background currents (solid lines) and without background currents (dashed lines) along the transects of 6.5°N (a), 10°N (b) and 13.5°N (c). The thick red lines represent the bathymetries along the transects.

compared the results discussed above with the results without considering background currents. Figures 5 and 7 (dashed lines) show the zonal distribution of linear parameters (c, β) along each transect when $U(z) = 0$. The results are similar to those presented in solid lines. The maximum phase speed is 2.5 m/s in the cool season. The dispersion parameters keep the same order of magnitude. The distribution of the phase speed and dispersion parameter still depend mainly on the topographic feature. However, without considering background currents, the difference between the results in rainy season and hot season shrinks.

The zonal distribution of nonlinear parameters (α, α_1) are shown in Figs 9 and 11 (dashed lines). Different from linear parameters, nonlinear parameters are greatly affected by the background flow. The quadratic nonlinear parameters fluctuate around –0.005 5 s^{-1} in the deep sea of the southern and northern AS. While in the central AS, the value of α is around –0.002 5 s^{-1} in the deep sea, it is almost half of the result of considering the background flow. In the shallow water, the results in different seasons vary a lot, especially in the northern AS. The cubic nonlinear parameters α_1 even change their signs. In the deep sea, the value of α_1 is around 5.5×10^{-4} m/s, much smaller than the result of considering the background flow, i.e., α_1 is reduced by approximately 1/3. Therefore, the background flow has a great influence on nonlinear parameters. In the deep sea, the absolute values of α and α_1 are smaller when $U(z) = 0$. In the shallow water area, the results vary greatly with seasons.

5 Conclusions

In the paper, the evKdV theory is used here to evaluate kinematic parameters of ISWs in the AS. The horizontally variable density stratification and background currents are taken into account in the evKdV theory. The temperature and salinity data are from SODA, and the background zonal velocities are from HYCOM. Based on these data, the phase speed, dispersion parameter, quadratic and cubic nonlinear parameters, and amplitude of ISWs in the AS are obtained. The phase speed and dispersion parameter are mainly determined by the topographic feature in the AS and have little seasonal variation. The phase speed can be up to 2.6 m/s in the cool season, and it is slightly larger in the cool season than those in the other two seasons, especially in the southern and central AS. In the cool season, the phase speed can be 11.4% larger than that in the rainy season. The dispersion

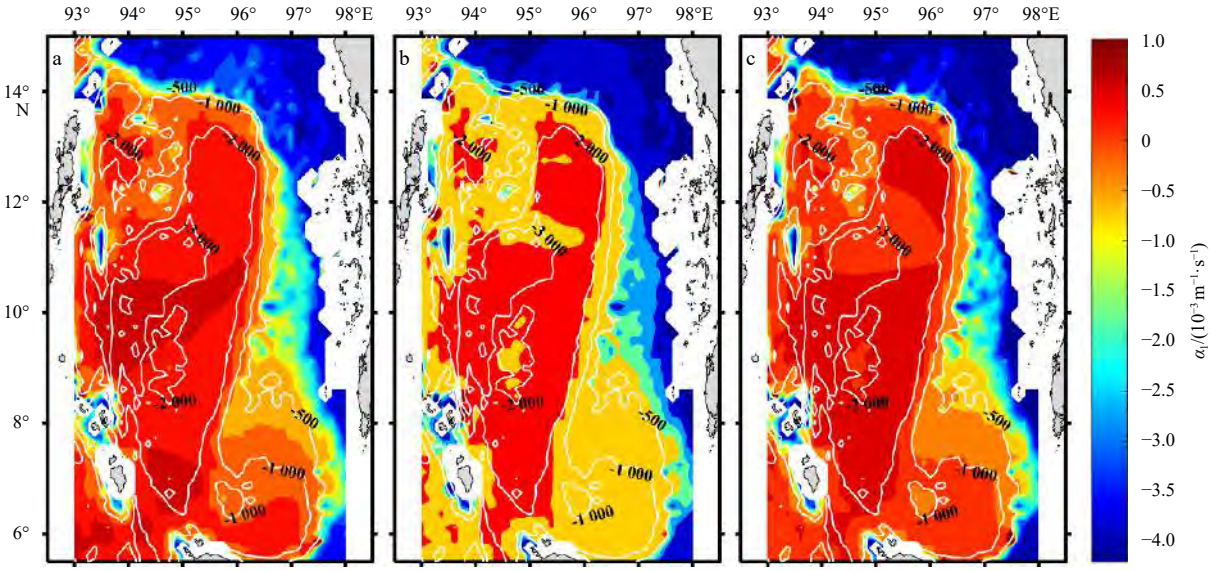

Fig. 10. Geographic distribution of the cubic parameter α_1 in March (a), July (b) and November (c). The white lines are isobaths in m.

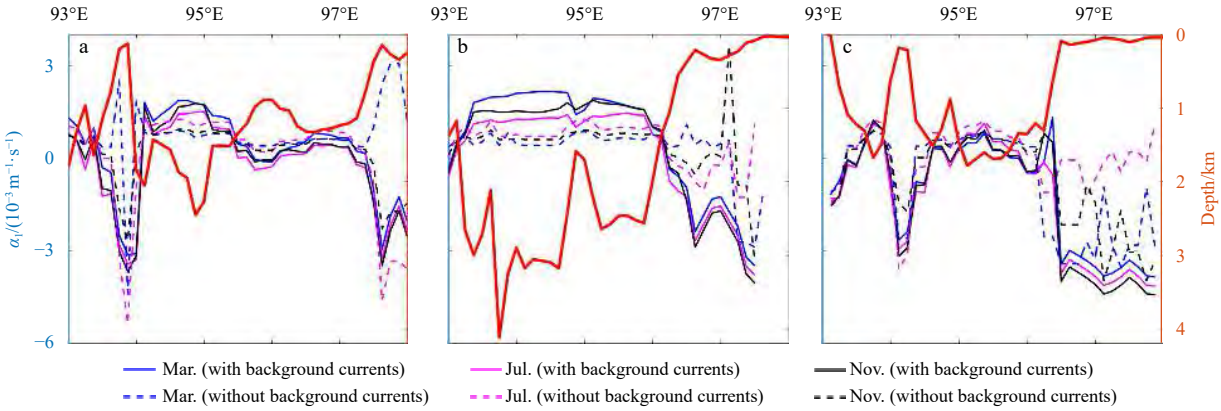

Fig. 11. Zonal distribution of the cubic parameter α_1 obtained by evKdV equation with background currents (solid lines) and without background currents (dashed lines) along the transects of 6.5°N (a), 10°N (b) and 13.5°N (c). The thick red lines represent the bathymetries along the transects.

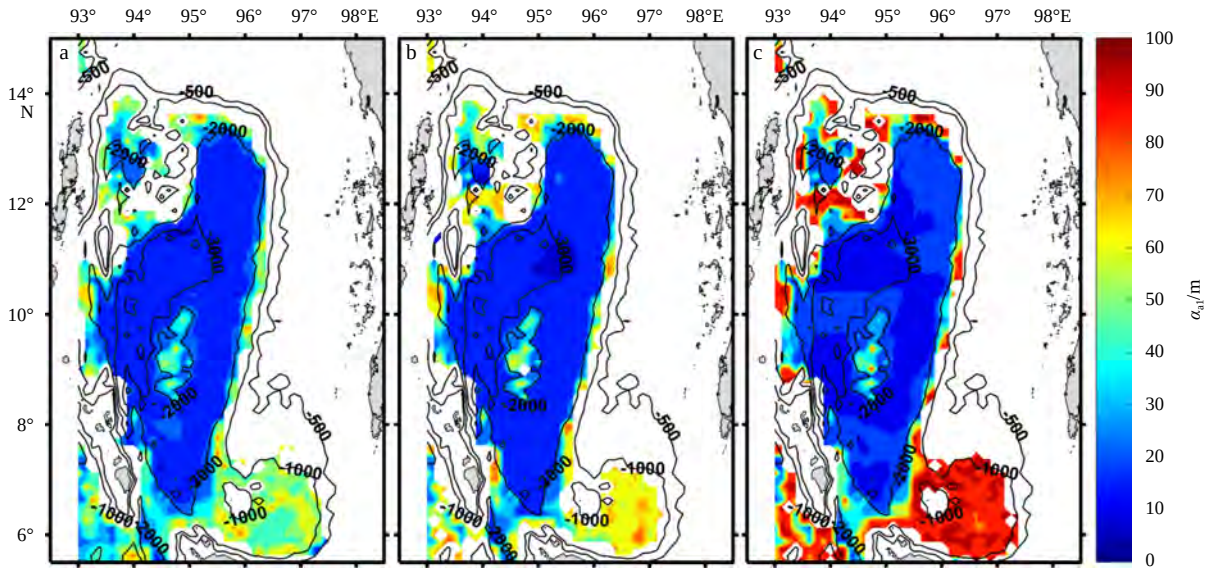

Fig. 12. Geographic distribution of algebraic solitons amplitudes a_{al} in March (a), July (b) and November (c). The black lines are isobaths in m.

parameter in the cool season can be 22.3% larger than that in the hot season. The quadratic and cubic nonlinear parameters have significant seasonal variation, these nonlinear parameters can change their signs at the continental slope in the AS, from season to season. In the deep sea, the value of the quadratic nonlinear parameter fluctuates around –0.005 5 s^{-1}. The cubic nonlinear parameter is negative in the shallow water and positive in the deep sea. Based on the nonlinear parameters, it is concluded that the algebraic solitons dominate in the AS, and the maximum a_{al} is 102 m, which happens in the cool season in the southern AS. To figure out the effect of background currents, we also calculate the linear and nonlinear parameters under the evKdV theory without considering background currents. The results show that background currents have little effects on the phase speed and dispersion parameter, but greatly change the quadratic and cubic nonlinear parameters. The nonlinear parameters vary greatly with seasons in the shallow water area without considering the background flow. The cubic nonlinear parameter can be reduced by 1/3 in the deep sea. The above conclusions are important to the deeply understanding of internal waves in the Andaman Sea.

Acknowledgements

We thank NOAA for providing high resolution topographic data from ETOPO1 Global Relief Model (https://www.ngdc.noaa.gov/mgg/global/global.html), IRI/LDEO Climate Data Library for providing SODA data (http://iridl.ldeo.columbia.edu/SOURCES/.CARTON-GIESE/.SODA/.v2p0p2-4/), and HYCOM (https://www.hycom.org/dataserver/gofs-3pt0/analysis).

References

Alpers W, Heng Wangchen, Hock L. 1997. Observation of internal waves in the Andaman Sea by ERS SAR. In: IGARSS'97.1997 IEEE International Geoscience and Remote Sensing Symposium Proceedings. Remote Sensing—A Scientific Vision for Sustainable Development. Piscataway: IEEE, 1518–1520

Apel J R, Thompson D R, Tilley D G, et al. 1985. Hydrodynamics and radar signatures of internal solitons in the Andaman Sea. John Hopkins APL Technical Digest, 6(4): 330–337

Benney D J. 1966. Long non-linear waves in fluid flows. Journal of Mathematics and Physics, 45(1–4): 52–63, doi: 10.1002/sapm196645152

Cai Shuqun, Xie Jieshuo, Xu Jiexin, et al. 2014. Monthly variation of some parameters about internal solitary waves in the South China Sea. Deep-Sea Research Part I: Oceanographic Research Papers, 84: 73–85, doi: 10.1016/j.dsr.2013.10.008

da Silva J C B, Magalhaes J M. 2016. Internal solitons in the Andaman Sea: A new look at an old problem. Remote Sensing of the Ocean, Sea Ice, Coastal Waters, and Large Water Regions 2016, 9999: 42–54

Grimshaw R. 2001. Internal solitary waves. In: Grimshaw R, ed. Environmental Stratified Flows. Boston: Kluwer, 1–28

Grimshaw R, Pelinovsky E, Poloukhina O. 2002. Higher-order Korteweg–de Vries models for internal solitary waves in a stratified shear flow with a free surface. Nonlinear Processes in Geophysics, 9(3–4): 221–235

Grimshaw R, Pelinovsky E, Talipova T, et al. 2004. Simulation of the transformation of internal solitary waves on oceanic shelves. Journal of Physical Oceanography, 34(12): 2774–2791, doi: 10.1175/JPO2652.1

Grimshaw R, Pelinovsky E, Talipova T, et al. 2010. Internal solitary waves: propagation, deformation and disintegration. Nonlinear Processes in Geophysics, 17(6): 633–649, doi: 10.5194/npg-17-633-2010

Holloway P E, Pelinovsky E, Talipova T. 1999. A generalized Korteweg-de Vries model of internal tide transformation in the coastal zone. Journal of Geophysical Research: Oceans, 104(C8): 18333–18350, doi: 10.1029/1999JC900144

Hyder P, Jeans D R G, Cauquil E, et al. 2005. Observations and predictability of internal solitons in the northern Andaman Sea. Applied Ocean Research, 27(1): 1–11, doi: 10.1016/j.apor.2005.07.001

Kakutani T, Yamasaki N. 1978. Solitary waves on a two-layer fluid. Journal of the Physical Society of Japan, 45(2): 674–679, doi: 10.1143/JPSJ.45.674

Kurkina O, Rouvinskaya E, Talipova T, et al. 2017a. Propagation regimes and populations of internal waves in the Mediterranean Sea basin. Estuarine, Coastal and Shelf Science, 185: 44–54

Kurkina O, Talipova T, Soomere T, et al. 2017b. Kinematic parameters of internal waves of the second mode in the South China Sea. Nonlinear Processes in Geophysics, 24(4): 645–660, doi: 10.5194/npg-24-645-2017

Lamb K G, Yan Liren. 1996. The evolution of internal wave undular bores: comparisons of a fully nonlinear numerical model with weakly nonlinear theory. Journal of Physical Oceanography, 26(12): 2712–2734, doi: 10.1175/1520-0485(1996)026<2712:TEOIWU>2.0.CO;2

Liao Guanghong, Xu Xiaohua, Liang Chujin, et al. 2014. Analysis of kinematic parameters of internal solitary waves in the northern South China Sea. Deep–Sea Research Part I: Oceanographic Research Papers, 94: 159–172, doi: 10.1016/j.dsr.2014.10.002

Magalhaes J M, da Silva J C B. 2018. Internal solitary waves in the Andaman Sea: new insights from SAR imagery. Remote Sensing, 10(6): 861, doi: 10.3390/rs10060861

Osborne A R, Burch T L. 1980. Internal solitons in the Andaman Sea. Science, 208(4443): 451–460, doi: 10.1126/science.208.4443.451

Perry R B, Schimke G R. 1965. Large-amplitude internal waves observed off the northwest coast of Sumatra. Journal of Geophysical Research, 70(10): 2319–2324, doi: 10.1029/JZ070i010p02319

Wang Juan, Yang Jingsong, Zhou Liying, et al. 2019. Distribution of internal waves in the Andaman Sea and its adjacent waters based on multi-satellite remote sensing data. Journal of Marine Sciences, 37(3): 1–11

Zhou Xianchi, Grimshaw R. 1989. The effect of variable currents on internal solitary waves. Dynamics of Atmospheres and Oceans, 14: 17–39, doi: 10.1016/0377-0265(89)90055-9

Zhou Liying, Yang Jingsong, Wang Juan, et al. 2016. Spatio-temporal distribution of internal waves in the Andaman Sea based on satellite remote sensing. In: 2016 9th International Congress on Image and Signal Processing, BioMedical Engineering and Informatics (CISP-BMEI). Piscataway: IEEE, 624–628